



# The 2023 Marine Heatwave In The North Atlantic Tropical ocean

Amélie Loubet<sup>1</sup>, Simon J. van Gennip<sup>1</sup>, Romain Bourdallé-Badie<sup>1</sup>, Marie Drevillon<sup>1</sup>

<sup>1</sup>Mercator Océan International, 2 Av. de l'Aérodrome de Montaudran, 31400, Toulouse, France

*Correspondence to:* Simon J. van Gennip (svangennip@mercator-ocean.fr)

## Abstract.

In a context of climate change, Marine Heat Waves (MHW) are becoming more intense, frequent and/or lasting longer. During the year 2023 and based on the Copernicus Marine forecast system, the Mercator Ocean International MHW bulletin (<https://www.mercator-ocean.eu/en/category/mhw-bulletin/>) highlighted week after week a MHW event occurring in the North Tropical Atlantic. In this paper, we propose an 4D characterisation of this event using the Copernicus Marine global reanalyses. We demonstrate how this MHW event in North Tropical Atlantic 2023 is extraordinary compared to previous years. All indices commonly used for characterising MHWs (intensity, duration, total activity and area) reached values not observed before both at the surface but also in subsurface. The timing and vertical structure differs across the basin, with MHWs developing first in the North-East, with peaks of severity in June and progressively moving south westward across the basin. A characterisation of MHWs at all vertical levels reveals that the vertical structure differs across subregions with different processes at play: in the Eastern and subtropical centre of the gyre heat propagates from the surface to the subsurface spanning beyond the mixed layer depth; whereas in the Caribbean region, abnormally warm waters at depth are transported from remote equatorial regions by eddies traversing the area.

## Short summary

Marine Heatwaves (MHWs) are intensifying due to climate change. In 2023, the Copernicus Marine forecast system tracked a significant MHW event in the North Tropical Atlantic. Here we show this event was unprecedented, at the surface and at depth. It peaked in the northeast in May, spreading southwest to reach the Caribbean by fall. In the east and centre, the MHW remained within the surface layers, while in the Caribbean, it reached deeper levels due to warm waters advected by equatorial eddies.



## 1 Introduction

The year 2023 was the warmest year on record with annual average global atmospheric temperature reaching  $1.43 \pm 0.11$  °C above pre-industrial levels (Foster et al., 2024). Air temperature records were broken for multiple months and regions (WMO, 2024). Europe and the subtropical North Atlantic region were particularly affected with warmest air temperature anomalies on records (ESOTC, 2023). Abnormally high temperature anomalies have also been detected at the surface of the ocean consistently across products (observation, forecasting system, reanalysis) in the North Atlantic where mean temperature estimates have exceeded those of previous years (Copernicus, 2024). A direct result of this warming ocean is the occurrence of extreme warm events.

When abnormally high ocean temperatures occur for a sustained period of time it leads to an extreme event referred to in the literature as Marine Heat Waves (MHW). A standardised MHW definition was proposed by Hobday et al. (2016, 2018), that has enabled to document in a standardised manner MHW characteristics such as MHW duration, intensity and extent globally. MHW frequency has already increased between 1925-2016 (Oliver et al. 2018) and will keep on increasing due to anthropogenic forcing (Frölicher et al., 2018 ; Oliver et al., 2019). MHWs threaten marine ecosystems causing harm from species to ecosystem level such as coral bleaching, reduction of habitat-forming seaweed, harmful algal blooms, species range shift and mass mortality events (Le Nohaïc et al., 2017; Wernberg et al., 2013, 2016 ; Smith et al., 2023 ; Cavole et al., 2016).

The regular monitoring of MHW conditions globally (MOi weekly bulletin) revealed the prolonged presence across the year of an MHW event within the North Atlantic basin. Studies documenting MHWs in the NA have only been local to regional, with no records of such widespread events occurring (Frölicher and Laufkötter, 2018; Smith et al., 2021; Zhang et al., 2023). Furthermore, MHW have been well studied for the surface where long satellite records exist, but description and understanding of their vertical structure remains incomplete.

Vertical structure has been studied using Argo data (El Zahaby and Schaeffer, 2019, 2021; Zhang et al., 2023) but such approach suffer from an incomplete and coarse reconstruction of a climatology to evaluate with accuracy MHW characteristics (based on the ability to determine a state when water temperature remains above a specific threshold e.g. the 90th percentile of a daily climatology). Alternative approaches consist in the use of a reanalysis (Darmaraki et al. 2019) which provide a continuous complete 3-dimensional ocean state but require the system to be data assimilating, eddy resolving, of daily resolution, and covering a sufficiently long period to build a reliable climatology. In addition, to enable the study of recent events, such reanalyses need to be regularly updated to remain close to real time.

We propose a 4-dimensional description (3D + time) of the ocean temperature extreme event of 2023 in the north tropical Atlantic using the temperature field of the Copernicus Marine Service GLORYS12V1 reanalysis product (Lellouche et al. 2021), to which Hobday's Marine Heatwave algorithm has been applied (Hobday et al. 2016, 2018). After the method



description in section 2, we propose, in section 3, a characterization of the 2023 event in the tropical north Atlantic, from the surface to the sub-surface. Conclusions and perspectives are done in section 4.

## 2 Methods

### 2.1 Datasets

Product Ref. No.	Product ID & type	Data Access	Documentation
1	GLOBAL_MULTIYEAR_PHY_001_030, numerical model	EU Copernicus Marine Service Product (2023)	Product User Manual (PUM): Drévillon et al., 2023a Quality Information Document (QUID): Drévillon et al., 2023b Journal article: Lellouche et al., 2021
2	ERA5 reanalysis	CLimate data store ( <a href="https://cds.climate.copernicus.eu">https://cds.climate.copernicus.eu</a> )	Hersbach, H., Bell, B., Berrisford, P., Hirahara, S., Horányi, A., Muñoz-Sabater, J., et al. (2020). The ERA5 global reanalysis. Quarterly Journal of the Royal Meteorological Society 146, 1999–2049. doi: 10.1002/qj.3803

**Table 1: Product reference table**

The main product used for this study is the GLOBAL\_MULTIYEAR\_PHY\_001\_030 reanalysis distributed by Copernicus Marine Service (<https://doi.org/10.48670/moi-00021>). This reanalysis is developed from the NEMO global ocean model with a horizontal resolution of 1/12° (9 km at the equator and 2 km close to the poles) and with 50 vertical levels where observational products are assimilated using a reduced-order Kalman filter. Along track altimeter data (Sea Level Anomaly), Satellite Sea Surface Temperature, Sea Ice Concentration and In situ Temperature and Salinity vertical Profiles are jointly assimilated. Moreover, a 3D-VAR scheme provides a correction for the slowly-evolving large-scale biases in temperature and salinity. This reanalysis covers the period 1993-onward. It was driven by the ERAinterim atmospheric fluxes from 1993 to 2019, then ERA5 thereafter. A more detailed description and study is proposed by Lellouche et al. 2020. The use of ocean reanalysis makes it possible to both study surface MHWs and to compare the results with other satellite datasets but also to have an in-depth view. This reanalysis is particularly well suited to the study of near-surface phenomena due to its refined vertical discretization in



the first 50 metres of the ocean. In this study we calculated the 30-year (1993-2022) 3D daily climatology of temperature, and used the data from the year 2023 to characterise the MHW in the Tropical North Atlantic.

## 2.2 Characterisation of Marine Heatwaves

We identified a MHW event as a period of at least five consecutive days where the temperature ( $T$ ) exceeds the 90th percentile ( $T_{90}$ ) of the 30-year climatology (Hobday et al., 2016). The 90th percentile is smoothed over a 31-day window ( $sT_{90}$ ) to detect MHW and to compute their intensity ( $I = T - sT_{90}$ ) and duration (number of consecutive days above  $sT_{90}$ ). We divided MHW into four categories based on intensity (Hobday et al., 2018): moderate ( $I < sT_{90} - T_{mean}$ ), strong ( $sT_{90} - T_{mean} \leq I < 2(sT_{90} - T_{mean})$ ), severe ( $2(sT_{90} - T_{mean}) \leq I < 3(sT_{90} - T_{mean})$ ) and extreme ( $4(sT_{90} - T_{mean}) \leq I$ ); where  $T_{mean}$  is the temperature climatology. We detected MHW from the surface to 2,225 m depth (41 depth layers) for 2023 and additionally at the surface from 1993 to 2022. We defined the studied area to focus on regions with long lasting MHWs, choosing the Atlantic from 10° S to 50°N.

We calculated the MHW activity, for each years, following Simon et al. (2022) definition:

$$\sum_{event \in year} meanIntensity_{event} * duration_{event \in year} * surface_{event}$$

where *event* refers to a specific MHW event, *year* refers to a specific year,  $meanIntensity_{event}$  (in °C) is the *event* intensity averaged over its duration,  $duration_{event \in year}$  (in days) is the *event* duration within the specific year and  $surface_{event}$  (in km<sup>2</sup>) is the spatial extent of the *event*. Here we calculated activity for each grid cell, so  $surface_{event}$  is the surface of the grid cell. Then we averaged the activity over the studied area to get the mean spatial activity.

We divided the study area into coherent subregions following the definition of the Longhurst biogeochemical provinces (shapefile from [Marine Regions · Longhurst Provinces \(Longhurst Province\)](#)). Based on the highest activity regions, we focus on the provinces denoted North Atlantic Subtropical Gyral Province (East) (NASE), North Atlantic Tropical Gyral Province (NATR), and Caribbean Province CARB (Figure2).

Daily MHW intensities used in time series and depth profiles were calculated with an unsmoothed 90th percentile. For time series, we spatially averaged the daily intensity over each chosen Longhurst province; for generating the mean vertical MHW intensity profiles, for each depth level we first temporally averaged the daily MHW intensity (using MHW days only) for each grid cell in the province, and then we spatially averaged the temporal mean values of each gridcell within the province.

## 2.3 Atmospheric Variables

Using ERA5 reanalysis air temperature ( $TAIR$ ) and 10m wind ( $U10$ ) data, we computed 2023 anomalies based on 30-year climatologies (1993-2022) to match the sea temperature climatology (used to detect MHWs). The air temperature anomaly



12 ( $TAIR - TAIR_{clim}$ ) was then smoothed over a 7-day window. For the wind at 10m, we calculated the anomaly of the absolute  
 13 values ( $|U10| - |U10_{clim}|$ ) to focus on anomalies of intensity and not of direction. Then the anomaly was averaged over  
 14 2023.

### 15 **3 Results**

#### 16 **An event of unprecedented characteristics at the surface**

17 During the year 2023 a MHW event of extraordinary characteristics occurred in the tropical North Atlantic impacting the entire  
 18 ocean region between 10 °S and 50 °N (Figure 1a). The event developed in March, covering ~20% of the region predominantly  
 19 in moderate conditions, to progressively peak from August to mid-October gaining in both extent and intensity occupying over  
 20 60% of the area, with strong and higher categories progressively accounting for nearly 60% of the MHW surface by mid  
 21 October (43.5% for strong, 14.8% for severe and 1.1% for extreme on 15th October). A decrease in extent occurred in October,  
 22 and in December with in between a slight increase in November (Figure 1b).

23 Overall, nearly the entire area (>99%) has been in MHW conditions at some point across the year, with such conditions going  
 24 beyond moderate in terms of category (Figure 2a). Indeed, only 8.3% of the region was exposed to moderate-only events  
 25 during the year, and corresponds to regions in the vicinity of the Gulf Stream and its extension. In total, 40.2% of the region  
 26 has been exposed to a maximum level of category strong, 40.7% of category severe, and 10.8% of category extreme and  
 27 beyond. The most intense events span from the Iberian peninsula, the eastern side of the basin and the Caribbean region.  
 28 Noteworthy, the regions with most intense MHW events (Figure 2a) coincide with region with highest number of marine  
 29 heatwave days (long lasting MHW areas of Figure 1a); for instance the region between 15°N and 35°N spanning from the East  
 30 of the African coast until 40 °W and the one close to Hispaniola island in the Caribbean region.

31 In terms of duration, a large proportion (19.9 % of the study region, mostly constrained within the triangle formed by the  
 32 Iberian peninsula, western Africa and the Caribbean region) was in MHW condition for more than 250 days during the year  
 33 (Figure 1a). Most notably, the region off the coast of Morocco was exposed to more than 300 MHW days. The Gulf Stream  
 34 region was more moderately impacted with around 100 MHW days over the year 2023.

35 The year 2023 is characterised by an unprecedented MHW event outstanding in all indices commonly used to describe MHWs  
 36 with highest mean daily intensity, mean duration, total surface exposed and total activity (Figure 1c). On average over a year,  
 37 2023 exceeds all previous years of the reanalysis product (1993-2022) with mean duration of 54 days over the area, mean daily  
 38 intensity of 0.52 °C and mean activity of 17,204 °C.day-1.km2 (Simon et al., 2022). No other year presents similar high values  
 39 for a single of these metrics (nevertheless all 3 combined) underlining the extraordinary nature of the 2023 MHW event. Note  
 40 that this extent corresponds to a strong negative anomaly in surface wind intensity.

41 The timing corresponding to the peak of the event in terms of MHW category (Figure 2b) varied geographically, with highest  
 42 category first reached during springtime in the eastern part of the basin, then during July/August for the centre of the basin,  
 43 and during fall for the western part.

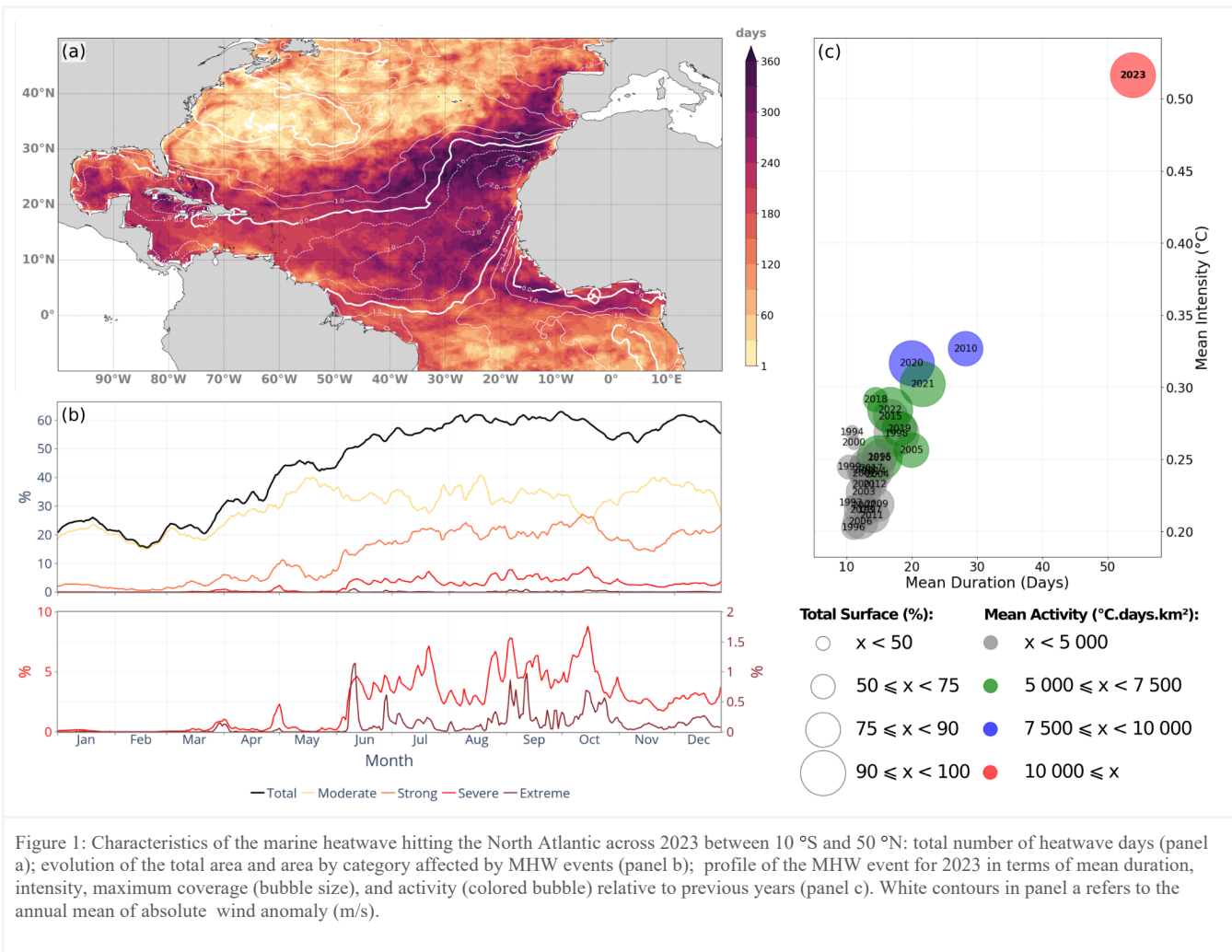


Figure 1: Characteristics of the marine heatwave hitting the North Atlantic across 2023 between 10 °S and 50 °N: total number of heatwave days (panel a); evolution of the total area and area by category affected by MHW events (panel b); profile of the MHW event for 2023 in terms of mean duration, intensity, maximum coverage (bubble size), and activity (colored bubble) relative to previous years (panel c). White contours in panel a refers to the annual mean of absolute wind anomaly (m/s).



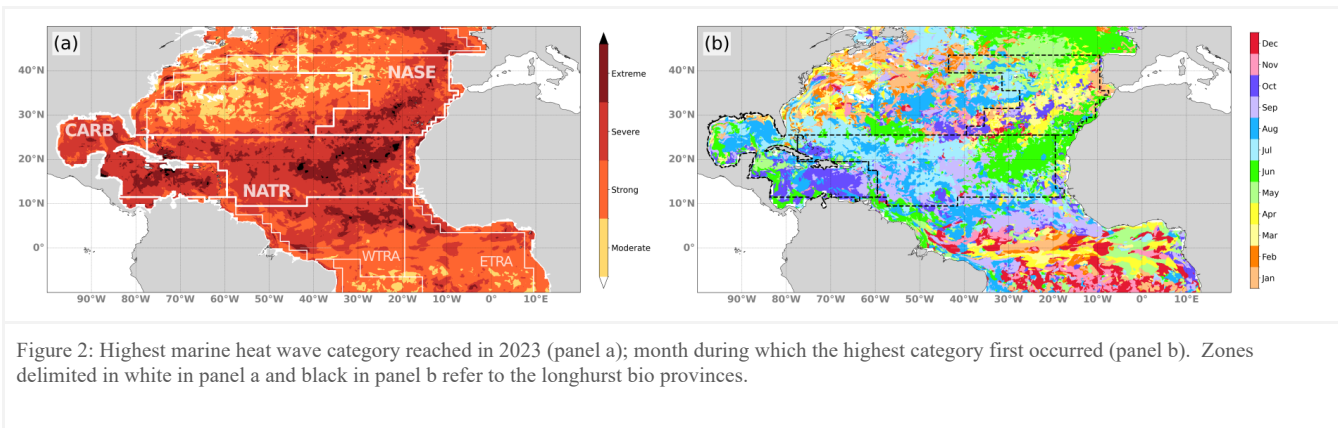


Figure 2: Highest marine heat wave category reached in 2023 (panel a); month during which the highest category first occurred (panel b). Zones delimited in white in panel a and black in panel b refer to the longhurst bio provinces.

### Regional vertical structure of MHW

Beyond the extraordinary surface signature of the 2023 MHW event, we further investigate this event by characterising its vertical structure and evolution over time. For this, we divided the study area into physically coherent subregions as defined by Longhurst (Reygondeau et al., 2013 ; Longhurst, 2007) (Figure 2a).

We focus on 3 subregions where intense and long MHW events occurred (Figure 1a, 2a): the North Atlantic Subtropical Gyral Province (NASE), to the east of the basin; the North Atlantic Tropical Gyral Province (NATR), in the centre; and Caribbean Province (CARB) to the west . For each subregion, we computed the mean intensity depth profile. For each depth, we first averaged for each gridcell the intensity from all heatwave days across the year, and then spatially averaged the mean temporal MHW intensity of each gridcell within the subregion.

The depth profile of MHW intensity is not identical across the basin, with significant differences across the region (Figure 3a), most notably for the depth where the maximum intensity occurred. Intensity peaks at much deeper depth in the CARB region (max at 155 m, deeper than the mean MLD of 23.8 m over the subregion), than for NASE and NATR regions, that show maxima at 40m and close to the surface, respectively, both within the mixed layer. The mean intensity profile of MHW for NASE shows homogeneous levels across the MLD with slightly higher values at subsurface (40.3 m depth) at the bottom of the mixed layer. The NATR region shows a different MHW intensity than the NASE region, with a maximum in the surface layer. In addition, we notice from the standard deviation of the MHW intensity that spatial inhomogeneity is largest for the CARB region for depth between 150 and 400m.



## Evolution of MHW Intensity and extent

Further insight on MHW characteristics was carried out by evaluating for each region the evolution of intensity and spatial extent of the MHW at depths (surface, 40m and 150m) where maximum intensity occurred in each region (Figure 3b,c and d).

At the surface, like observed in MHW highest categories (Figure 2b), later timing in the peak of MHW for the more westward regions is evidenced in the area averaged intensity. Maximum intensity is reached earlier in the most eastern the NASE region (beginning of may) then in the NATR region (late July), and in the CARB region (October)(Figure 3 a b & c, blue lines).

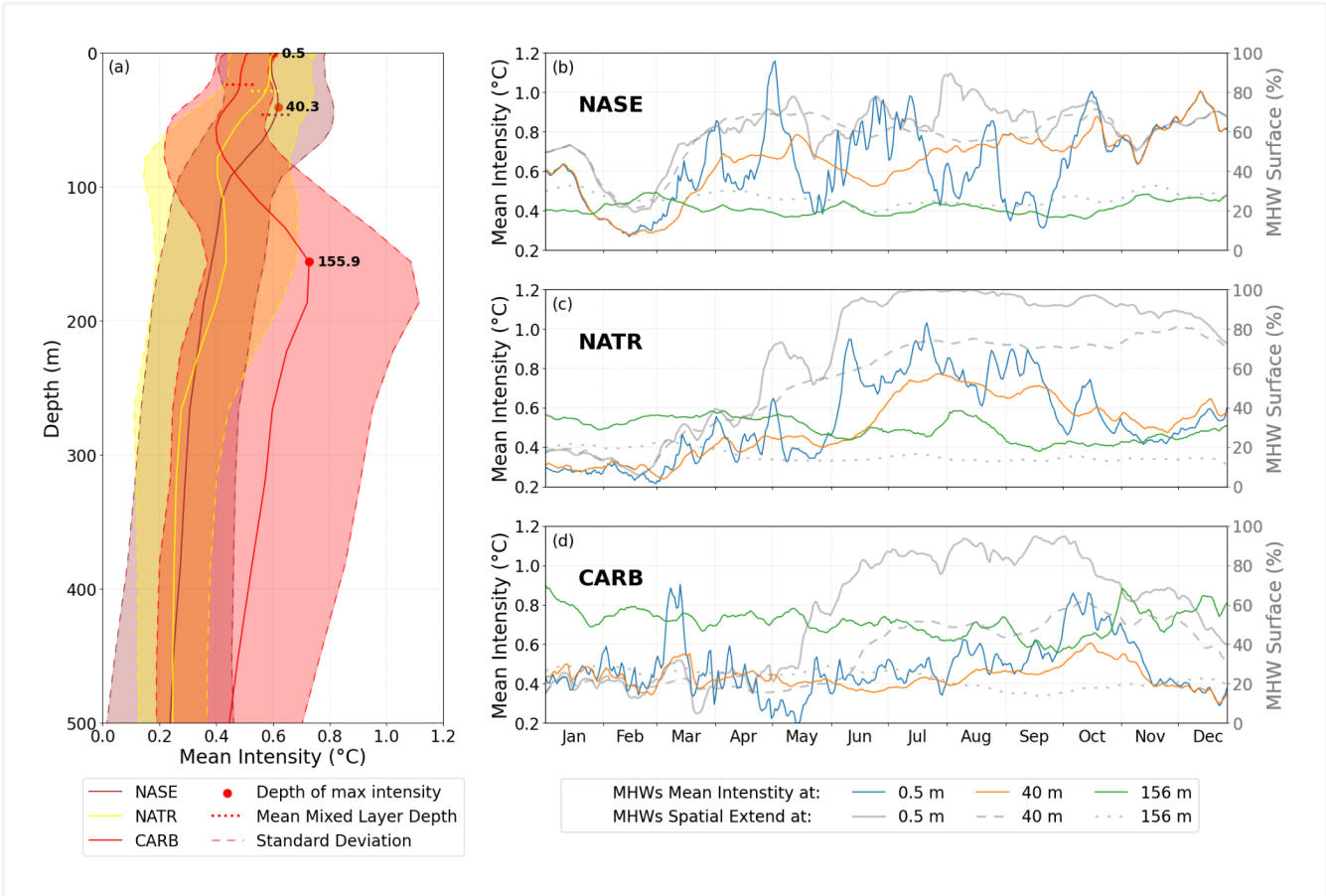


Figure 3: evolution of the intensity and surface coverage of the 2023 marine heatwave for different regions in the North Atlantic. Mean daily MHW intensity profile (a) of NASE (brown), NATR (yellow) and CARB (red). Shading areas represent standard deviations. Red dots represent depth of highest mean intensity. Time series of mean intensity (in °C) and surface coverage (in %) in NASE (b), NATR (c) and CARB (d) provinces. Colored lines represent the mean intensity at the surface (blue), at 40m (orange) and at 150m (green). Black lines represent the surface coverage at the surface (dashed), at 40m (dotted) and at 150m (solid).





81 For the NASE region, the intensity at the surface shows large fluctuations across the year: in total, six maxima of intensity  
 82 higher than  $0.8^{\circ}\text{C}$  are observed followed by low troughs (with differences of  $0.3$  to  $0.8^{\circ}\text{C}$  relative to the peaks). The intensity  
 83 at  $40\text{ m}$  depth – where maximum occurs in the mean depth profile – increases progressively from  $0.3^{\circ}\text{C}$  early March to peak  
 84 mid December at  $1.0^{\circ}\text{C}$ . In between some variations exist with smaller peaks mid may and mid october (occurring shortly  
 85 after the surface peaks). It suggests that the MHW signature at the surface is propagating through the mixed layer with response  
 86 at depth to atmospheric forcing not as fast than at the surface. Unlike shallower depths, the intensity at  $150\text{ m}$  remains stable  
 87 around  $0.4^{\circ}\text{C}$  across the year. In between  $40\text{ m}$  and  $150\text{ m}$  however, surface warming propagates progressively at depth across  
 88 the year. For instance at  $100\text{ m}$  depth, from February onwards the intensity levels steadily increase from values of  $0.29^{\circ}\text{C}$  to  
 89  $0.61^{\circ}\text{C}$  by mid-November (see Figure 4e).

90 Similarly, the increase in area occupied by MHWs for both the surface and  $40\text{ m}$  depth coincides with the shoaling of the MLD  
 91 (not shown). The horizontal extent is similar for both depths, with values fluctuating around  $70\%$  of the area from April to  
 92 mid-October. Extent is lower at  $150\text{ m}$  depth with values remaining between  $20\%$  to  $30\%$ .  
 93 The MLD deepening in October to levels deeper than  $40\text{ m}$  lead to more homogeneous MHW intensity and extent at the surface  
 94 and  $40\text{ m}$ .

96 The evolution of the mean intensity for NATR describes a different kind of MHW than for the NASE region. The MHW is  
 97 characterised by one long temporal event – rather than a series of shorter events – that peaks at the end of July. At the surface,  
 98 high intensity develops rapidly early June and remains high until the end of September with values constantly above  $0.5^{\circ}\text{C}$ .  
 99 Horizontal extent of the MHW increases in two steps: first reaching  $\sim 70\%$  at the end of April-May and then above  $90\%$  from  
 100 mid June to November, to finally drop slightly below  $80\%$ .

101 At  $40\text{ m}$  depth, rapid increase in intensity occurs later relative to the surface starting end of May at  $0.4^{\circ}\text{C}$  to reach a maximum  
 102 of  $0.77^{\circ}\text{C}$  by the end of July. Spatial extent increases progressively from  $\sim 40\%$  coverage in April to above  $80\%$  by the end  
 103 of November. At  $150\text{ m}$  depth, intensity levels vary across the year around  $0.4$ - $0.6^{\circ}\text{C}$ . Horizontal extent of MHW remains low  
 104 and stable across the year with coverage of  $15$ - $20\%$ . Unlike for the surface, no impact can be seen of the surface atmospheric  
 105 signature.

107 Dynamics for the CARB region differ with the NASE and NATR regions, with an MHW signal at both surface and depth . At  
 108 the surface, a late and long lasting peak of MHW intensity (larger than  $0.6^{\circ}\text{C}$  for  $30$  days) occur in October ( $0.86^{\circ}\text{C}$ ), after  
 109 the observed peaks in the other 2 regions. In addition, an short event is observed early March (lasting  $10$  days and reaching  
 110 an intensity of  $0.9^{\circ}\text{C}$ ). At  $40\text{ m}$ , intensity levels and fluctuations are similar to the surface, with lower magnitude and reduced  
 111 high frequency variations. Timing in the peaks in March and October show a lag relative to the surface. MHW horizontal  
 112 extent at the surface increases from  $\sim 30\%$  mid-May to peak late september to reach  $95\%$  of the area, to then decrease to  $\sim 40\%$   
 113 by the end of the year. Similar pattern can be seen at  $40\text{ m}$  depth with an increase in surface occurring later (mid-june) and  
 114 peaking mid-October at  $\sim 60\%$  to drop to  $\sim 30\%$  by the end of the year.



At 150 m – corresponding to the maximum intensity in the mean profile –, unlike for the other two regions, intensity levels are higher than levels reached for shallower depths. The intensity is stable and ranges between 0.6 °C and 0.8 °C for the entire year and is always higher than shallower depth except for October when a surface marine heatwave develops. High levels are however not widespread across the subregion as the surface exposed to MHWs remains around 20 % across the year. Noteworthy, sub-monthly variations are present in the MHW intensity timeseries suggestive of advective transient features like eddies crossing the domain.

### **MHW westward and vertical evolution**

Analysis of MHW within the 3 subregions of the NA, suggests that MHW surface signature propagates westward, and at depth. To further investigate such dynamics and potential drivers, a 3-dimensional decomposition along longitude, depth and time of the MHW intensity field and its possible drivers is carried out. The figure 4 (a,b,c) shows the evolution of MHW across the year and our study region using a Hovmöller diagrams with a latitudinal averaging of the intensity over the 3 regions and for the 3 different depths at which intensity maxima occurs in the 3 regions (surface, 40 m and 150 m).

For the surface, the strongest intensity (greater than 0.5°C) takes place primarily in the eastern half of the region (between 60 °W and 10 °W) and during the months of May to December (Figure 4a). This surface signature of the MHW can be directly associated with atmospheric features as large daily air temperature anomalies are observed which coincide in time and space with the MHW patterns (Figure 4d). This suggests a direct response of the surface ocean to the atmospheric anomaly. The eastern part is characterised by a larger number of peaks from march to december (as seen in the MHW intensity time series for the NASE subregion Figure 3b), whereas moving westwards to the central part of the region, the period of high intensity is reduced to the July to October period forming a single large spatio-temporal peak. Furthermore, we note that the pronounced intensity patterns in the eastern part (anomalies larger than 0.75 °C) propagate rapidly westward, most notably between 10 °W and 70 °W at velocity of ~1 m/s, starting in July and occurring nearly every month. To the west (70 °W to 100 °W), fast west propagation from signal in the central part of the basin can be observed in October. Further west than 80 °W a period of strong MHW intensity (July to October) coincides with a period of strong positive air temperature anomalies.

The patterns of intensity at 40 m depth relate strongly with patterns at the surface, namely large intensity in the Eastern half of the region spanning from April to December (Figure 4b). Peaks in intensity are smaller than for the surface, and patterns contain less high frequency signal. Similarly to the surface, multiple peaks in intensity characterise the eastern part and a single long event the central one (30 °W - 50 °W).

The similarity of the MHW signature at 40 m with the surface suggests that the atmosphere driving the MHW at the surface also reaches deeper layers. This correlation is confirmed by a depth/time Hovmöller of the NASE region (figure 4e). Across the period from March to November, the region is exposed to several high peaks in MHW intensity (Figure 3b) at the surface. These propagate rapidly across the mixed layer which vary from 100 m to 20 m in depth between winter and summer seasons.



.49 This propagation in the vertical also extends below the mixed layer depth. MHW Intensity larger than  $0.5^{\circ}\text{C}$  can be observed  
.50 below the MLD from April onwards with 70 m depth in April and progressively reaching 100 m by November. The  
.51 propagation across the MLD is rapid with a velocity ( $\sim 4$  m/day). Below the MLD, the propagation is slower ranging between  
.52  $0.7$ - $1.3$  m/day. A direct consequence is that the MHW-driven heat accumulation is trapped below the MLD to remain within  
.53 the ocean interior and be advected far away from the formation area.

.54  
.55 At 150 m depth, patterns in MHW intensity are very different to what is observed at the surface. On the eastern side, there is  
.56 no clear signature with only low MHW intensity levels. To the west, MHW intensity also differs with the surface, but unlike  
.57 the east some small spatial scale patterns emerge: west of  $70^{\circ}\text{W}$  and for the period of September to November, intensity  
.58 displays a diagonal showing MHW intensity propagating westward with a velocity of  $\sim 0.1\text{ m.s}^{-1}$ . Such westward velocity is  
.59 characteristic of the eddies crossing the Caribbean Basin (Richardson, 2005; Cailleau et al., 2024) suggesting such features are  
.60 responsible for the intense MHW conditions locally as they trap and carry westward abnormally warm waters. A snapshot of  
.61 the MHW intensity on the 7th July 2023 at 150 m overlaid with the Sea Surface Heights anomaly confirms the intensity  
.62 anomalies are trapped in the anticyclonic eddies at depth in this region (figure 4f).

.63 These very strong local anomalies (larger than  $2^{\circ}\text{C}$  above the q90 threshold) are limited in space, and explain the low and  
.64 stable horizontal extent of MHWs in the CARB region at 150 m depth (Figure 3d). Part of such anomalies come from the  
.65 NATR region, but predominantly from the Equatorial and North Brazil currents located below the NATR region (e.g. the  
.66 eddies located at  $57^{\circ}\text{W}$ - $10^{\circ}\text{N}$  on figure 4f). A detailed study of this region is necessary to understand the processes but falls  
.67 beyond the range of our study area and would also require a longer study period spanning beyond 2023 as MHW anomalies  
.68 are still strongly present in 2024 at the equator.

.69  
.70

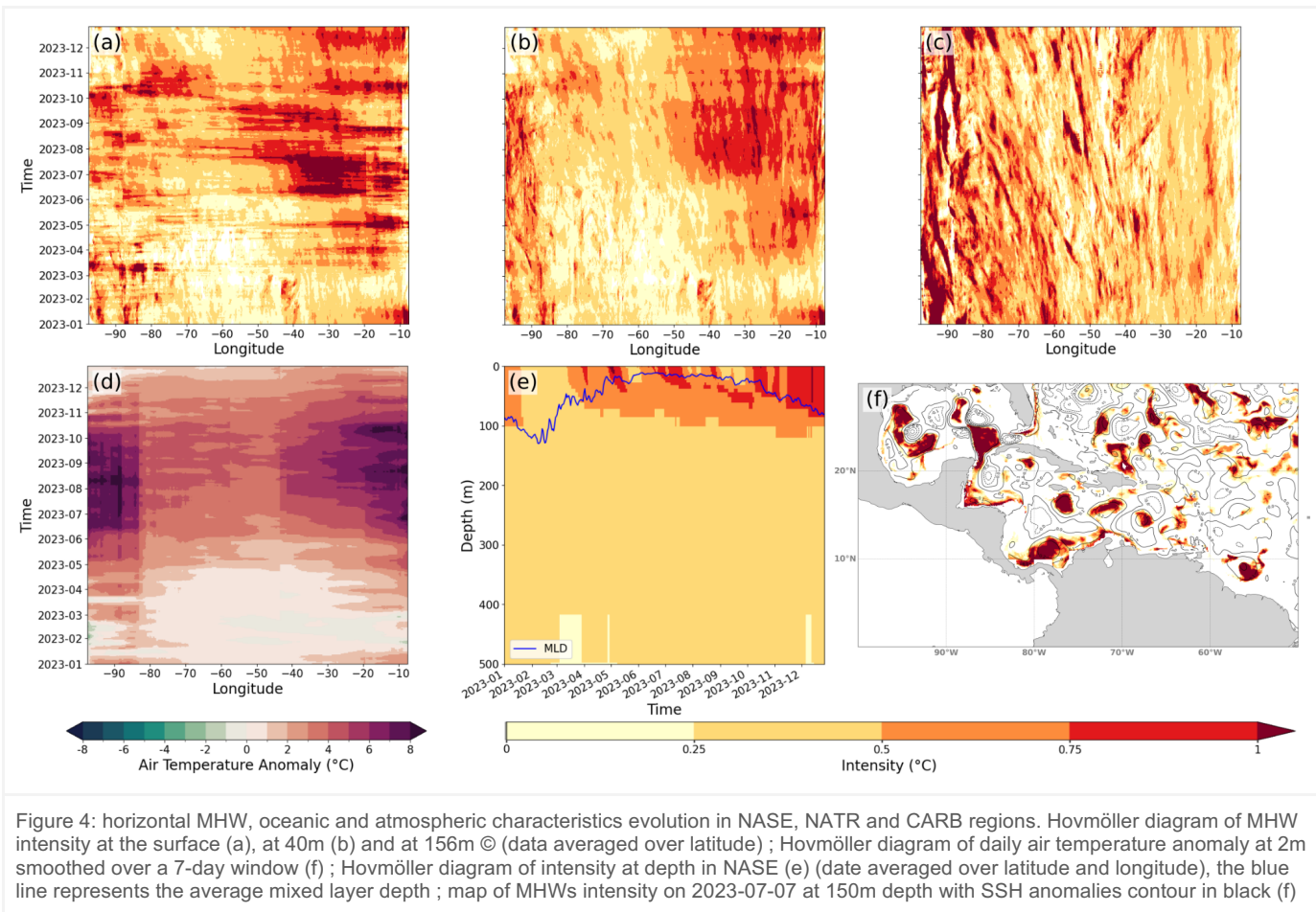


Figure 4: horizontal MHW, oceanic and atmospheric characteristics evolution in NASE, NATR and CARB regions. Hovmöller diagram of MHW intensity at the surface (a), at 40m (b) and at 156m © (data averaged over latitude) ; Hovmöller diagram of daily air temperature anomaly at 2m smoothed over a 7-day window (f) ; Hovmöller diagram of intensity at depth in NASE (e) (date averaged over latitude and longitude), the blue line represents the average mixed layer depth ; map of MHWs intensity on 2023-07-07 at 150m depth with SSH anomalies contour in black (f)

## 4 Discussion and conclusions

Various meteorological and oceanographic estimates showed that the year 2023 was exceptional in terms of heat record, and in particular the tropical North Atlantic. We therefore applied a Marine Heat Wave detection algorithm commonly used in the community (Hodday et al. 2016) to this region using data from the Copernicus marine global reanalysis product. The use of the reanalysis allowed us to perform detection both at the surface and at depth. Compared to previous years, we show the exceptional nature of 2023 in the tropical North Atlantic. The detected surface MHW surpasses the last 30 years in terms of duration, intensity and coverage. A strong link with surface atmospheric conditions is shown (air temperature, negative trade wind anomaly). We also noted an evolution of the maxima during the year with a predominance in the East of the basin during the months of May to June then an evolution of this maximum anomaly towards the West to wait for the Caribbean Sea in



September. A decomposition into different areas of interest for marine biology (Longhurst zone), and an in-depth study on these areas highlighted the vertical propagation deeper and deeper towards the West and a progressive penetration of the MHW under the Mixed Layer Depth in the Eastern part. The intensification of the anomaly under the MLD is done progressively during the year. This is a remarkable phenomenon which can be potentially important because it induces a transport into the ocean interior of heat anomalies following surface extremes events. The Caribbean Sea region shows very strong MHW signal yet very localised in the subsurface, with a maximum around 150m. These anomalies characteristic of heat trapping eddies come partly from the North Tropical Atlantic but mainly from the North Brazil Current. A dedicated study on eddy-trapped heat pathways to the ocean interior should be considered in the future but will have to cover beyond the year 2023 because in the tropical zone (2°N-2°S), MHWs are still ubiquitous in 2024.

Also, a more comprehensive and detailed quantification of the different contributions of ocean and atmospheric processes is needed to thoroughly understand this unprecedented event. An approach based on the reconstruction of the heat equation could be done for which the use of the reanalysis would be instrumental namely to have access to a gridded 3D field on at a frequency of 1 day and as such limit errors due to the non-linearity of the equation and the approximation of the estimation of the depth of the mixed layer.

In view of the exceptional general characteristics of the MHW of 2023 in the tropical North Atlantic, further studies are needed, for example to quantify the impact on marine biogeochemistry (BGC), a study for which a BGC reanalysis of Copernicus Marine can be used (GLOBAL\_MULTIYEAR\_BGC\_001\_029), but also on the distribution of Sargassum algae – which have a strong societal harmful power – that develop largely in the Gulf of Guinea and are advected as far as the Caribbean region (Jouanno et al., 2021).

In addition, the definition of extremes could be regionalized and tailored to be representative of harm towards key local species. In this study, the potential of ocean reanalyses to characterise a specific event was shown. Further work on the the detection and analysis of extremes would be of interest to assess the MHW impact and importance on the more general climate context. Heat from this North Atlantic MHW propagates under the mixed layer to reach different depths depending on the region. Such strong anomalies once away from the surface and trapped within subsurface water masses can potentially be advected over long distances, like the heat anomalies observed in this study at the equator that then got advected to the Caribbean region, the Gulf of Mexico and potentially back into the North Atlantic through the Gulf Stream. Detection and monitoring of extremes over the 30 years of the reanalysis will enable to propose an initial scheme and an initial quantification of the importance of such extremes on the overall ocean interior heat content. This estimate will then have to be compared to data sets with a longer time period in order to validate the hypotheses deduced from the study of the GLORYS12 reanalysis fields.

## Acknowledgements

We would like to thank the Ocean State Report team for the insightful comments and advice in developing of this manuscript



#### Author contribution

SJVG and RBB led the conceptualization of the study, the analysis and writing of the manuscript. AL performed the simulations, data analysis and writing of the manuscript. MD contributed to the conceptualization of the study, and reviewing the manuscript.

#### Competing interests

The authors declare that they have no conflict of interest.

#### References

Copernicus publication. Copernicus. Record high global sea surface temperatures continue in August | Copernicus: <https://climate.copernicus.eu/record-high-global-sea-surface-temperatures-continue-august>.

ESOTC. Copernicus Climate Change Service (C3S). « European State of the Climate 2023 ». Copernicus Climate Change Service (C3S), 2024. <https://doi.org/10.24381/BS9V-8C66>.

Cailleau, S., Bessi res, L., Chiendje, L., Dubost, F., Reffray, G., Lellouche, J.-M., van Gennip, S., R gnier, C., Drevillon, M., Tressol, M., Clavier, M., Temple-Boyer, J., and Berline, L.: CAR36, a regional high-resolution ocean forecasting system for improving drift and beaching of *Sargassum* in the Caribbean archipelago, *Geoscientific Model Development*, 17, 3157–3173, <https://doi.org/10.5194/gmd-17-3157-2024>, 2024.





- 32 Darmaraki, S., Somot, S., Sevault, F., and Nabat, P.: Past Variability of Mediterranean Sea Marine Heatwaves,  
33 <https://doi.org/10.1029/2019GL082933>, n.d.
- 34 Elzahaby, Y. and Schaeffer, A.: Observational Insight Into the Subsurface Anomalies of Marine Heatwaves, *Front. Mar. Sci.*,  
35 6, <https://doi.org/10.3389/fmars.2019.00745>, 2019.
- 36 Elzahaby, Y., Schaeffer, A., Roughan, M., and Delaux, S.: Oceanic Circulation Drives the Deepest and Longest Marine  
37 Heatwaves in the East Australian Current System, <https://doi.org/10.1029/2021GL094785>, n.d.
- 38 Forster, P. M., Smith, C., Walsh, T., Lamb, W. F., Lamboll, R., Hall, B., Hauser, M., et al. « Indicators of Global Climate  
39 Change 2023: Annual Update of Key Indicators of the State of the Climate System and Human Influence ». *Earth System*  
40 *Science Data* 16, no 6 (5 juin 2024): 2625–58. <https://doi.org/10.5194/essd-16-2625-2024>.
- 41 Frölicher, T. L. and Laufkötter, C.: Emerging risks from marine heat waves, *Nat Commun*, 9, 650,  
42 <https://doi.org/10.1038/s41467-018-03163-6>, 2018.
- 43 Frölicher, T. L., Fischer, E. M., and Gruber, N.: Marine heatwaves under global warming, *Nature*, 560, 360–364,  
44 <https://doi.org/10.1038/s41586-018-0383-9>, 2018.
- 45 Grose, S. O., Pendleton, L., Leathers, A., Cornish, A., and Waitai, S.: Climate Change Will Re-draw the Map for Marine  
46 Megafauna and the People Who Depend on Them, *Front. Mar. Sci.*, 7, <https://doi.org/10.3389/fmars.2020.00547>, 2020.
- 47 Hobday, A. J., Alexander, L. V., Perkins, S. E., Smale, D. A., Straub, S. C., Oliver, E. C. J., Benthuyssen, J. A., Burrows, M.  
48 T., Donat, M. G., Feng, M., Holbrook, N. J., Moore, P. J., Scannell, H. A., Sen Gupta, A., and Wernberg, T.: A hierarchical  
49 approach to defining marine heatwaves, *Progress in Oceanography*, 141, 227–238,  
50 <https://doi.org/10.1016/j.pocean.2015.12.014>, 2016.
- 51 Hobday, A. J., Oliver, E. C. J., Gupta, A. S., Benthuyssen, J. A., and Burrows, M. T.: Categorizing and Naming Marine  
52 Heatwaves, *Oceanography*, 31, 162–173, <https://doi.org/10.5670/oceanog.2018.205>, 2018.
- 53 Jouanno, J., Benshila, R., Berline, L., Soulié, A., Radenac M. H., Morvan, G., Diaz, F., et al. « A NEMO-Based Model of  
54 *Sargassum* Distribution in the Tropical Atlantic: Description of the Model and Sensitivity Analysis (NEMO-Sarg1.0) ». *Geoscientific Model Development* 14, n° 6 (1 juillet 2021): 4069–86. <https://doi.org/10.5194/gmd-14-4069-2021>.



- 56 Lellouche, J.-M., Greiner, E., Bourdallé-Badie, R., Garric, G., Melet, A., Drévillon, M., Bricaud, C., Hamon, M., Le Galloudec,  
57 O., Regnier, C., Candela, T., Testut, C.-E., Gasparin, F., Ruggiero, G., Benkiran, M., Drillet, Y., and Le Traon, P.-Y.: The  
58 Copernicus Global 1/12° Oceanic and Sea Ice GLORYS12 Reanalysis, *Front. Earth Sci.*, 9,  
59 <https://doi.org/10.3389/feart.2021.698876>, 2021.
- 60 Le Nohaïc, M., Ross, C. L., Cornwall, C. E., Comeau, S., Lowe, R., McCulloch, M. T., and Schoepf, V.: Marine heatwave  
61 causes unprecedented regional mass bleaching of thermally resistant corals in northwestern Australia, *Sci Rep*, 7, 14999,  
62 <https://doi.org/10.1038/s41598-017-14794-y>, 2017.
- 63 Longhurst, A. R.: *Ecological Geography of the Sea*, <https://doi.org/10.1016/B978-0-12-455521-1.X5000-1>, 2007.
- 64 Oliver, E. C. J., Donat, M. G., Burrows, M. T., Moore, P. J., Smale, D. A., Alexander, L. V., Benthuisen, J. A., Feng, M., Sen  
65 Gupta, A., Hobday, A. J., Holbrook, N. J., Perkins-Kirkpatrick, S. E., Scannell, H. A., Straub, S. C., and Wernberg, T.: Longer  
66 and more frequent marine heatwaves over the past century, *Nat Commun*, 9, 1324, [https://doi.org/10.1038/s41467-018-03732-](https://doi.org/10.1038/s41467-018-03732-9)  
67 [9](https://doi.org/10.1038/s41467-018-03732-9), 2018.
- 68 Oliver, E. C. J., Burrows, M. T., Donat, M. G., Sen Gupta, A., Alexander, L. V., Perkins-Kirkpatrick, S. E., Benthuisen, J. A.,  
69 Hobday, A. J., Holbrook, N. J., Moore, P. J., Thomsen, M. S., Wernberg, T., and Smale, D. A.: Projected Marine Heatwaves



- 70 in the 21st Century and the Potential for Ecological Impact, *Front. Mar. Sci.*, 6, <https://doi.org/10.3389/fmars.2019.00734>,  
71 2019.
- 72 Reygondeau, G., Longhurst, A., Martinez, E., Beaugrand, G., Antoine, D., and Maury, O.: Dynamic biogeochemical provinces  
73 in the global ocean, *Global Biogeochemical Cycles*, 27, 1046–1058, <https://doi.org/10.1002/gbc.20089>, 2013.
- 74 Richardson, P. L.: Caribbean Current and eddies as observed by surface drifters, *Deep Sea Research Part II: Topical Studies*  
75 in Oceanography, 52, 429–463, <https://doi.org/10.1016/j.dsr2.2004.11.001>, 2005.
- 76 Simon, A., Plecha, S. M., Russo, A., Teles-Machado, A., Donat, M. G., Auger, P.-A., and Trigo, R. M.: Hot and cold marine  
77 extreme events in the Mediterranean over the period 1982–2021, *Front. Mar. Sci.*, 9,  
78 <https://doi.org/10.3389/fmars.2022.892201>, 2022.
- 79 Smith, K. E., Burrows, M. T., Hobday, A. J., Sen Gupta, A., Moore, P. J., Thomsen, M., Wernberg, T., and Smale, D. A.:  
80 Socioeconomic impacts of marine heatwaves: Global issues and opportunities, *Science*, 374, eabj3593,  
81 <https://doi.org/10.1126/science.abj3593>, 2021.
- 82 Smith, K. E., Burrows, M. T., Hobday, A. J., King, N. G., Moore, P. J., Gupta, A. S., Thomsen, M. S., Wernberg, T., and  
83 Smale, D. A.: Biological Impacts of Marine Heatwaves, *Annual Review of Marine Science*, 15, 119–145,  
84 <https://doi.org/10.1146/annurev-marine-032122-121437>, 2023.
- 85 Wernberg, T., Smale, D. A., Tuya, F., Thomsen, M. S., Langlois, T. J., De Bettignies, T., Bennett, S., and Rousseaux, C. S.:  
86 An extreme climatic event alters marine ecosystem structure in a global biodiversity hotspot, *Nature Clim Change*, 3, 78–82,  
87 <https://doi.org/10.1038/nclimate1627>, 2013.
- 88 Wernberg, T., Bennett, S., Babcock, R. C., de Bettignies, T., Cure, K., Depczynski, M., Dufois, F., Fromont, J., Fulton, C. J.,  
89 Hovey, R. K., Harvey, E. S., Holmes, T. H., Kendrick, G. A., Radford, B., Santana-Garcon, J., Saunders, B. J., Smale, D. A.,  
90 Thomsen, M. S., Tuckett, C. A., Tuya, F., Vanderklift, M. A., and Wilson, S.: Climate-driven regime shift of a temperate  
91 marine ecosystem, *Science*, 353, 169–172, <https://doi.org/10.1126/science.aad8745>, 2016.



92 World Meteorological Organization. WMO confirms that 2023 smashes global temperature record:  
93 <https://wmo.int/news/media-centre/wmo-confirms-2023-smashes-global-temperature-record>,

94 Zhang, Y., Du, Y., Feng, M., and Hobday, A. J.: Vertical structures of marine heatwaves, Nat Commun, 14, 6483,  
95 <https://doi.org/10.1038/s41467-023-42219-0>, 2023.

96

97 **Supplementary materials**

98 No SP

99